Using Spectral methods to numerically solve the Nonlinear Dirac Model

lxxqiu001

April 2023

Abstract

The Nonlinear Dirac model is a complex model that appears in many fiedls of Physics. It also happens that the solutions to this model cannot be found numerically. This report provides a brief overview on the Nonlinear Dirac Model and how Spectral methods can be used to approximate its' solutions. The system is also further analysed to compute the long-term stability of its solution waves. The various behaviours the waves can take on are also shown and analysed.

Contents

1 Introduction

Models can be used to describe physical systems in many fields, such as mechanics as well as electromagnetism. The solution to many of these systems often cannot be computed analytically and are thus computed numerically. Many of these models cannot be computed numerically due to nonlinear terms in the equations.

The nonlinear coupled Dirac Model is one of these models that cannot be computed analytically. This paper will provide a brief overview of the Dirac Model as well as methods that can be used to compute its time evolution numerically. The space derivative of the system will be computed using spectral methods, a class of accurate and simple numeric approximation techniques. Time derivatives will be approximated using standard integrators to time evolve the system.

The accuracy and efficiency of the integrators will be analysed and compared. The resulting behaviour of the numeric solutions satisfying the Dirac model will also be discussed. Before we may begin searching for a numeric solution to the Dirac Model, we must understand what the Dirac Model is, as well as what it defines.

2 What is Dirac?

The Dirac Equation is one of the central equations of Relativistic Quantum Mechanics. (Xu et al, 2013). It was originally formulated to describe electron-spin and more generally the fermion spin. The Dirac Equation is also a wave equation, illustrating the wave-particle duality property of matter in QM.
The simple (1+1) linear Dirac Model is shown in equation 1 where u and v are two scalar fields.

$$i(u_x + u_t) + v = 0 \tag{1}$$

The interaction between these fields can be coupled by nonlinear terms which results in the system of equations shown in equation 2.

$$\begin{aligned} i(u_t + u_x) + v + |v|^2 u = 0 \\ i(v_t - v_x) + u + |u|^2 v = 0 \end{aligned} \tag{2}$$

The functions u and v that will satisfy 2 can be found numerically. The functions u, v will be soliton solutions known as Spinors that do not change shaoe over time. The Dirac Model shown above is of a special form, representing the wave function of two fermions with opposite spins. The full Dirac Model is system of complex equations that usually requires a deep understanding of both physics and mathematics to interpret. We will therefore turn to an alternative method to simplify the explanation of what the Dirac Model is.

2.1 A conversation with ChatGPT

ChatGPT is a large language model that has proven to be an excellent tool for research in many industries. Although it performs poorly when doing calculations, it excels in providing information about certain topics. We use ChatGPT to provide a background on the Dirac Models and its' solutions.

2.1.1 What is the Dirac Model

"The Dirac model is a theoretical framework for describing the behavior of electrons in a relativistic setting, developed by British physicist Paul Dirac in 1928. The model combines the principles of special relativity and quantum mechanics to describe the behavior of electrons moving at speeds close to the speed of light.

One of the key features of the Dirac model is the prediction of the existence of antiparticles. Dirac realized that the equations describing the behavior of relativistic electrons could have solutions that corresponded to negative energy states. He interpreted these solutions as representing particles with the same properties as electrons, but with opposite charge. These particles, now known as positrons, were later discovered experimentally.

The Dirac equation, which describes the behavior of electrons in the Dirac model, is a relativistic wave equation that takes into account both the spin and the charge of the electron. It predicts that electrons have two possible spin states, and it accurately describes a range of phenomena, including the fine structure of atomic spectra and the behavior of electrons in magnetic fields."

The Dirac model has had a profound impact on modern physics, and it is a key component of the Standard Model of particle physics, which describes the behavior of all known particles and their interactions.

This is a comprehensive description of the Dirac Model with no explicitly incorrect facts. The Dirac Model obviously has more applications and deeper complexities, however in the context of this report, this information is sufficient.

2.1.2 What are Spinors?

"Spinors are mathematical objects used in physics to describe the behavior of particles with intrinsic angular momentum, or "spin." They were first introduced by the mathematician Élie Cartan in the 1910s as a way to extend the theory of rotations to include half-integer values of the spin.

Spinors are used extensively in modern physics, particularly in quantum field theory and particle physics, where they are used to describe the behavior of fundamental particles such as electrons and quarks. They also play a role in general relativity, where they are used to describe the behavior of fermions in curved spacetime."

This description of Spinors is correct and provides a brief overview of their history as well as their applications, however, the fact that Spinors are Solitons is not mentioned. The Mathematical properties of Spinors are ommitted completely from this description.

2.1.3 How can we time evolve Spinors?

"The time evolution of the Spinor can be found by solving the Dirac equation, which is a partial differential equation. In general, this is a difficult problem to solve analytically, and numerical methods are often used to solve the equation. One common numerical method is the finite difference method, which involves approximating the derivatives in the equation by finite differences and using iterative methods to solve the resulting system of equations.

Once the spinor is known, the time evolution of observables such as the spin and energy can be calculated using the appropriate operators. The spin operator is given by the Pauli matrices, and the energy operator is given by the Hamiltonian operator, which takes into account the kinetic and potential energy of the electron.

Spinors are characterized by their transformation properties under rotations. When a spinor is rotated by a certain angle, it does not return to its original state, but rather picks up a phase factor, which is related to the spin of the particle. In this way, spinors capture the essential feature of quantum mechanics that particles can have intrinsic angular momentum, and that the act of measuring this angular momentum can fundamentally alter the state of the system."

A method to time evolve of these Spinor solutions is not explicitly given in ChatGPT's Response. The Chatbot has opted to provide the some information about Spinor properties and behaviours but fails to explicitly explain how these Spinors can be evolved over time. We will thus

2.2 Stationary State solutions

The time independent form of (2) is simply (3) without the time derivative. This system will have solutions Φ, and Ψ.

$$\begin{aligned} -i\Phi_x + w\Phi + \Psi + |\Psi|^2\Phi = 0 \\ i\Psi_x + w\Psi + \Phi + |\Phi|^2\Psi = 0 \end{aligned} \tag{3}$$

Φ and Ψ are soliton solutions which are known as Spinors. These solitons are propogating waves that maintain their shape and speed after interacting with another wave. The equation of these Spinor solitons is shown in (4)

$$\begin{aligned} \Phi(x) = \frac{K}{cosh(kx + i\alpha)} \\ \Psi(x) = \frac{-K}{cosh(kx - i\alpha)} \end{aligned} \tag{4}$$

The coefficicients in 3 4 are shown in 5. The value of α will not change the form of the stationary state waves Φ and Ψ.

$$\begin{aligned} 0 < \alpha < \frac{\pi}{2} \\ w = cos(2\alpha) \\ k = \sqrt{1 - w^2} \end{aligned} \tag{5}$$

The initial form of the two solitons is shown in figure 1. The solitons are plotted in the interval $x \in [-\pi, \pi]$. These waves are periodic since $\Phi(-\pi) = \Phi(\pi) = 0$ and $\Psi(-\pi) = \Psi(\pi) = 0$. This property of the Soliton will be useful later when constructing methods to differentiate the solutions.

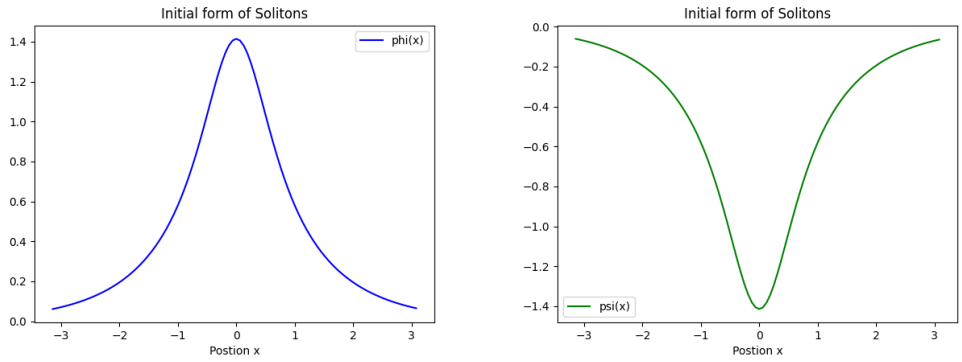

Figure 1: Initial trajectories of $\Phi(x), \Psi(x)$

The Spinors of form (4) satisfy the time independent Dirac Solution. In order to show this, we will implement a simple iteration to show that hump solutions such as the ones seen in Figure 1, will satisfy the equations (3). We begin by rewriting (3) in differential form shown in (6).

$$\begin{aligned} \Phi_x = -i(w\Phi + \Psi + |\Psi|^2\Phi) \\ \Psi_x = i(w\Psi - \Phi - |\Phi|^2\Psi) \end{aligned} \tag{6}$$

The simple iteration method we will use will be Runge-Kutta 4 where we evolve the system over several x-steps to get the value of Φ and Ψ at each x-point. If we take 900 x-steps with each stepsize$\Delta x = 0.01$, the approximate solutions Φ and Ψ are shown in Figure 2.

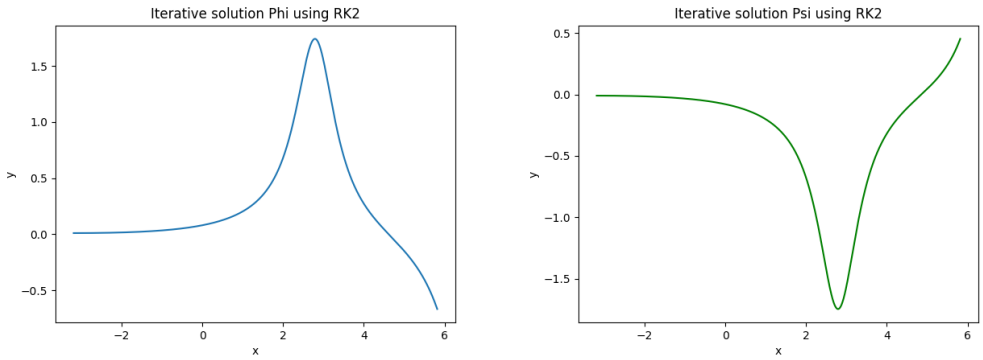

Figure 2: Initial trajectories of $\Phi(x), \Psi(x)$

This illustrates that there exist Hump solutions that will satisfy the time independent Dirac Model (3). The Spinors are therefore stationary state solutions that satisfy equation 3, however they will not satisfy the Complete Dirac model 2. The solutions to the Complete Model can be produced by evolving the Spinors Φ and Ψ over time, using a time operator e_{-iwt}. The solutions to the full Dirac model are shown below.

$$\begin{aligned} u(x,t) &= \Phi(x)e^{-iwt} \\ v(x,t) &= \Psi(x)e^{-iwt} \end{aligned} \tag{7}$$

The behaviour of these waves u, v over time can be approximated numerically. In order to do so, both the time and space derivatives of the solutions must be approximated. We will first consider methods to approximate the space derivative of the solutions. A common method to do this is by using Spectral methods.

3 Spectral Differentiation Matrices

The analytic derivative of $\Phi(x)$ and $\Psi(x)$ is shown in 8.[1] The functions would be difficult to compute for many timestep, since it has two hyerbolic trigonometric functions as well as real and imaginary parts.

$$\begin{aligned} \Phi'(x) &= -k^2 sech(kx + i\alpha)tanh(kx + i\alpha) \\ \Psi'(x) &= -k^2 sech(kx - i\alpha)tanh(kx - i\alpha) \end{aligned} \tag{8}$$

Since the analytical function is computationally expensive to compute, we can use numeric methods to approximate the derivative at each timestep. A class of numerical techniques known as Spectral methods are particularly suited to these problems.
Spectral methods are a group of techniques that can be used to solve PDEs accurately and efficiently. One of these methods can be used to approximate the derivative of a function using Differentiation matrices. These are matrices that act on functions to produce accurate approximations of the derivative. The accuracy of the approximations are determined by analysing the relative error of the approximations. The Differentiation matrices can be computed in two ways, using Fourier Transforms and Chebyshev Polynomials.

3.1 Fourier differentiation matrix

Given some periodic function $u(x)$, we can approximate the differentiation matrix using the Discrete Fourier Transforms (DFT). This Transform is shown in equation 9.

$$\hat{V_k} = h\Sigma_{j=1}^{N} v_j e^{-ikhj} \tag{9}$$

[1] In this section, α has been kept constant at $\alpha = \frac{\pi}{4}$ even though it will not influence the stationary state solitons.

The first step in constructing the differentiation matrix is discretising and bounding x. Since the function is periodic, $x \in [-\pi, \pi]$ with $x_0 = -\pi$,$x_N = \pi$, where N is the total number of x-points. The interval between each point will be $h = \frac{2\pi}{N}$. The continuous function itself is then also discretized via $u(x_j = v_j)$. Note that since $u(x)$ is periodic, $v_0 = v_N$. The discretised function v, is used to construct a band-limited interpolant shown in equation 10.

$$p(x) = \frac{1}{2}\Sigma_{k=\frac{-N}{2}}^{\frac{N}{2}} e^{ikx}\hat{V_k} \tag{10}$$

where $\hat{v_k}$ is the DFT shown in equation 9.

$p(x)$ is chosen in this form so that $p'(x)$ (We will denote $p'(x) = w_j$ for the sake of simplicity) will be real. This form of the interpolant can be simplified using the periodic sinc S_n function shown in equation 12, along with its' derivative.

$$p(x) = \Sigma_{m=1}^{N} \hat{V_m} S_N(x - x_m) \tag{11}$$

Equation 10 can be differentiated to produce w_j, which is an approximation of the derivative of $u(x,t)$. Differentiating $p(x)$ in its original form (Equation 10) is difficult, however this has been simplified using equation 12. Differentiating $p(x)$ in this form is equivalent to differentiating the Sinc function.

$$\begin{aligned} S_N(x_j) &= \frac{h}{2\pi}\frac{sin(\frac{Nx_j}{2})}{tan\frac{x_j}{2}} \\ S'_N(x_j) &= \frac{1}{2}(-1)^j cot(\frac{hj}{2}) \end{aligned} \tag{12}$$

Using equation 11, the w_j can produced as shown below.

$$w_j = p'(x) = \Sigma_{m=1}^{N} v_m S_n(x - x_m) \tag{13}$$

w_j can be written many forms. If we write equation 13 in matrix form, the differentiation matrix will be obtained. The matrix form can be interpreted as a simplified form of equation 12, where $\overrightarrow{V}$ is the vector with elements $v(x_j)$, D_N is the differentation matrix of size $N \times N$ and $\overrightarrow{W}$ is the derivative of the function at each point x_j.

$$\overrightarrow{W} = D_N \overrightarrow{V} \tag{14}$$

The differentiation matrix shown in equation 14 has elements produced using the formula:

$$SD(x_{mj}) = \begin{cases} 0 & m = j \\ \frac{1}{2}(-1)^{(m-j)} \frac{cot(h(m-j)}{2}) & m \neq j \end{cases} \tag{15}$$

where m is the row number, and j is the column number.

The Fourier Differentiation Matrix can be used to approximate the derivative of the Spinor solitons. The approximation of the derivative of $\Phi(x)$ and the accuracy of the approximation is shown below where $N = 20$ x points are used.

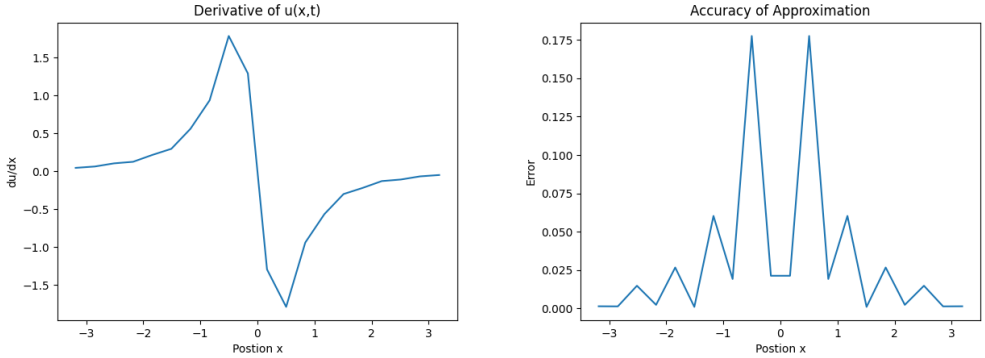

Figure 3: Approximate derivative of $\Phi(x)$ using Fourier and its accuracy when N=20

The derivative in Figure 3 is not smooth, and consequently may be quite inaccurate for many parts of the function. In order to smooth the approximation, we can use more x points. Figure 4 shows the approximate derivative where $N = 100$ x-points are used.

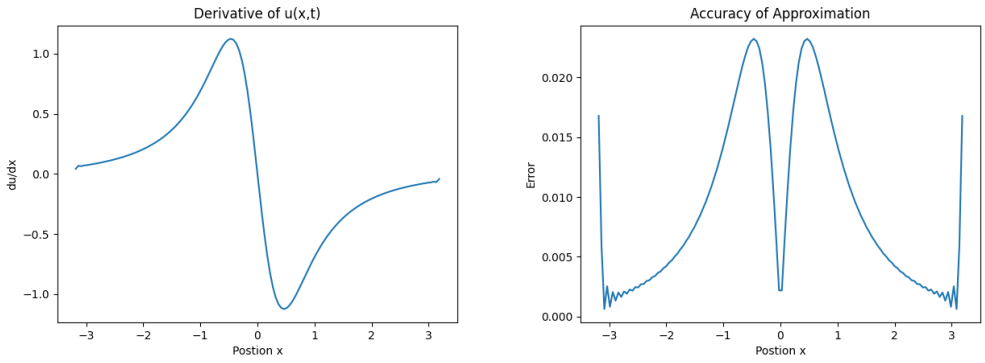

Figure 4: Approximate derivative of $\Phi(x)$ using Fourier and its accuracy when N=100

Figure 4 shows a smoother function, however the error of the approximation is still quite high. The error for both functions is of the magnitude 10^{-2}. The error does not decrease when more x points are used. We will therefore take $N = 100$, when using Fourier Differentiation matrices in relation to the solutions u, v to the Dirac Model.
The Fourier Approximations illustrates Runge Phenomena at the edges in both figure 3 and 4. This is where the approximation of a function becomes incredibly inaccurate. This is often due to even-spaced x-points. In order to reduce the effect of Runge Phenomena, we can use Chebyshev points which are not equidistant. We can rescale the system by a factor of L to reduce the error at the endpoints. For all uses of the Fourier Differentiation matrices in this report, $L = 5$ will be used to reduce the prevalence of RUnge Phenomena.

3.2 Chebyshev differentiation matrix

Chebyshev differentiation matrix is used to find the derivative of bounded non-periodic functions. The method is based on approximating the function using a Chebyshev Polynomial. We can begin this method by first defining the Chebyshev points

$$x_j = cos(\frac{j\pi}{N}) \; j = 0, 1...N \tag{16}$$

These points should Cluster near the bounds resulting in more accurate approximations since Runge Phenomena is less likely to occur. Given a function $u(x,t)$, the function is discretized via $u(x_j) = v_j$. Lagrange interpolation is then used on the discretized points v_j to produce a polynomial $p(x)$.
The Lagrange polynomial of order N will generate a Chebyshev Differentiation matrix D_N of size $N \times N$. The elements of D_N are shown in equation 17.

$$D_N(x_{i,j}) = \begin{cases} \frac{2N^2+1}{6} & i = j = 0 \\ \frac{-x_j}{2(1-x_j^2)} & i = j \\ \frac{c_i}{c_j}\frac{(-1)^{i-j}}{x_i - x_j} & i \neq j \\ -\frac{2N^2+1}{6} & i = j = N \end{cases} \tag{17}$$

The variables c_i, c_j are determined via

$$c_m = \begin{cases} 2 & m = 0, N \\ 1 & otherwise \end{cases} \tag{18}$$

Using this Matrix on Spinor solitons produces extremely accurate approximations of the derivative. The derivative Φ' and its accuracy is shown below in figure 5.

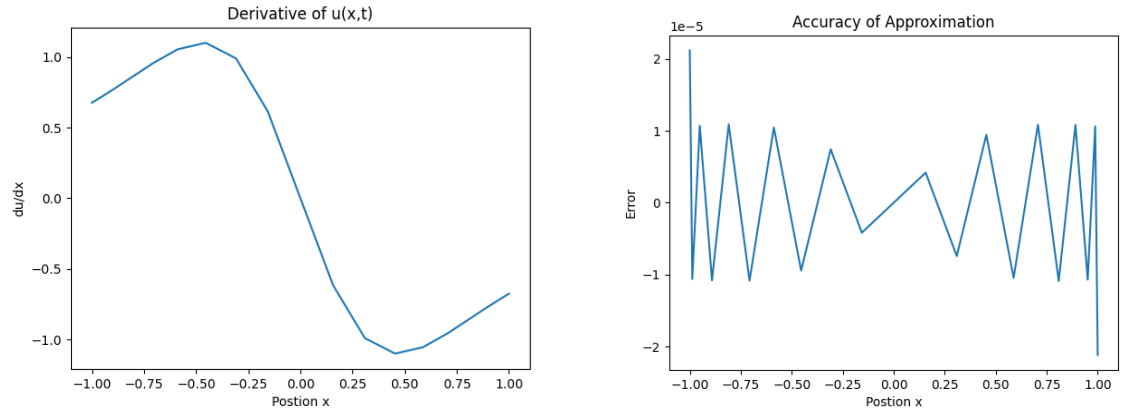

Figure 5: Approximate derivative of $\Phi(x)$ using Chebyshev and its accuracy when N=20

The approximation is not entirely smooth when $N = 20$ x-points, however the accuracy of the approximating is already more accurate than the Fourier approximation using $N = 100$ x-points. The Chebyshev approximation of Φ' using $N = 100$ points is shown in Figure 5. This will produce an even more approximation with an error of the magnitude 10^{-10}.

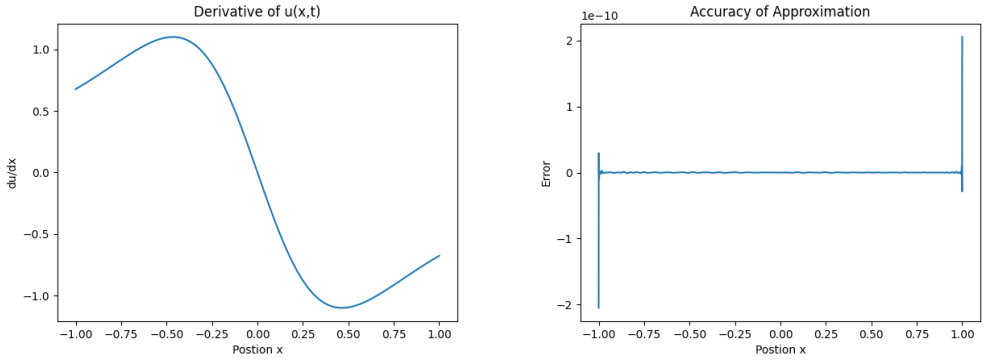

Figure 6: Approximate derivative of $\Phi(x)$ using Chebyshev and its accuracy when N=100

The blow up in error at the end points of the approximation are due to computational errors, since the endpoints are computed to be infinitely large or small. Removing the endpoints will result in an approximation with an accuracy of 10^{-12}, where the error oscillates similar to that of Figure 5.

The Chebyshev Differentiation Matrix produces a more accurate approximation of the derivative of a function compared to the Fourier Differentiation Matrix. Both Differentiation Matrices have certain properties that make them more appealing to use under certain conditions. We will illustrate this by using the less accurate Fourier Differentiation Matrix to approximate the solutions u and v over time.

4 Time Evolution of Spinors

The behaviour of the Spinors over time will vary depending on the value of parameter α. The Spinors $\Phi(x)$ and $\Psi(x)$ are evolved over time through the time operator e^{-iwt} to produce the time evolved solutions to the full Dirac model (2). These time evolved solutions cannot be computed analytically due to the nonlinear coupling that occurs between the two solitary waves. The u_x, v_x terms in 2 can be approximated using both Chebyshev and Fourier differentiation matrices. This report will only time evolution of Spinors using Fourier Differentiation matrices since the Chebyshev differentiation matrix tends to be unstable when evolving the approximations over time. The x interval is rescaled by a factor of $L = 5$ to reduce the effect of Runge Phenomena on the

approximation.

The Time derivative of the solutions u, v can be computed using two different methods, leapfrog and Runge-Kutta. The two methods will be compared for numeric accuracy and efficiency to evaluate which algorithm is better suited to the Dirac Models. We have previously mentioned that the value of α does not influence the stationary state solutions, however, this parameter will influence the behaviour of the Spinors as they evolve over time. The time evolution of the Spinors based on various α values will also be compared to illustrate the possible behaviours of the Spinors over time.

4.1 The LeapFrog integrator

The Leapfrog integrator approximates the time derivative using the formula shown in equation 19. This formula is substituted into equation 2 and rearranged to produce two equations that will evolve u and v.

$$u_t = \frac{u(x, t+1) - u(x, t-1)}{2\Delta t} \tag{19}$$

The Leapfrog method will be used with $\Delta t = 0.01$ to evolve Spinors in Figure 7. Warmer colours indicate that the Spinor is taking on positive values, whereas cool colours indicate negative values. The Spinors will have $\alpha = \frac{\pi}{4}$, which is known to produce stable waves. The Spinors are approximated using $N = 100$ x-points and evolved for 200 timesteps. The result in smooth Spinors as the system evolves.

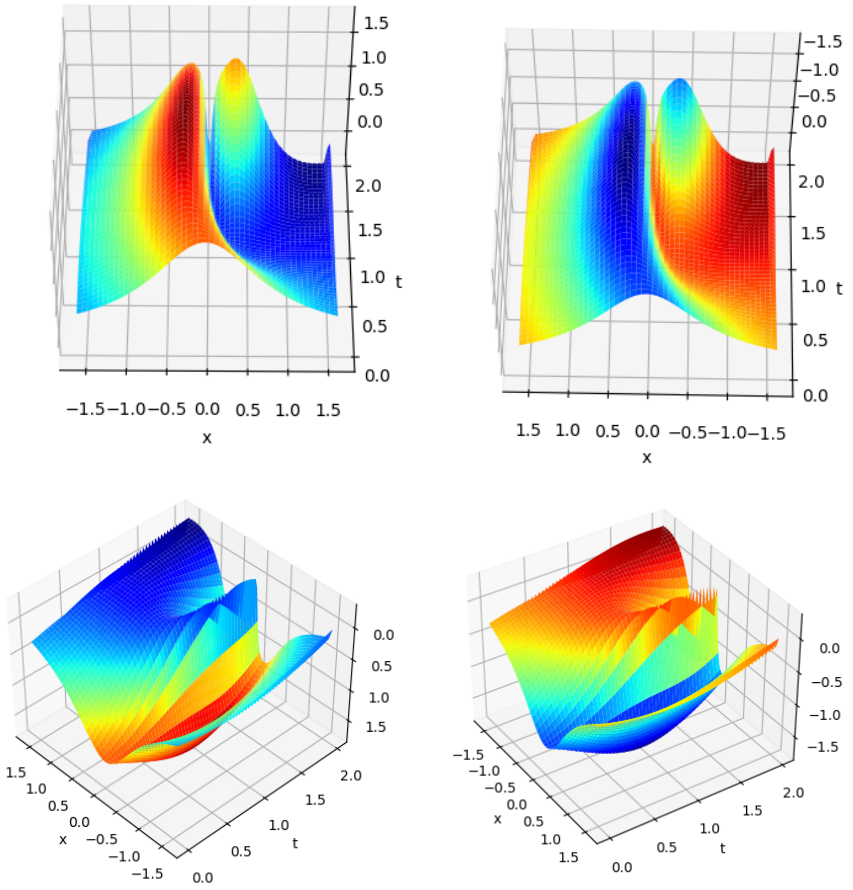

Figure 7: Time evolution of $u(x, t)$ *(left)* and $v(x, t)$ *(right)* using a LF integrator

In order to evolve the system over longer periods, we can either increase the Δt, or we can evolve the system over more timesteps. If we increase the Δt to 0.05, but keep all the other parameters used in Figure 7 the same,

the system will simply blow up. This is shown in Figure 8. This is largely due to stability conditions of the system and the eigenvalues λ that will be discussed in the next section.

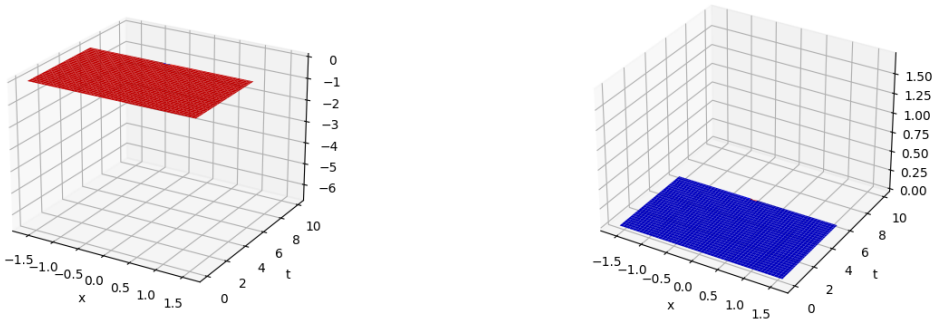

Figure 8: Time evolution of $u(x,t)$ *(left)* and $v(x,t)$ *(right)* using a LF integrator and a Fourier differentiation matrix

We will therefore retain that $\Delta t = 0.01$ to maintain the stability of the system. If we take $\alpha = \frac{\pi}{3}$, $N = 100$ and maintain $\Delta t = 0.01$ Figure 9 is produced. The evolution of the system will be mostly smooth with some minor spikes when the Spinors alternate their magnitude. The spikes are more likely the result of errors in the approximation of the system, rather than the actual beahviour of the spinors.

Both Figure 7 and 9 show that the system produces two solutions u, v that propogate in opposite directions. The magnitude and propogation direction are exact opposites, resulting in two anti-symmetric solutions.

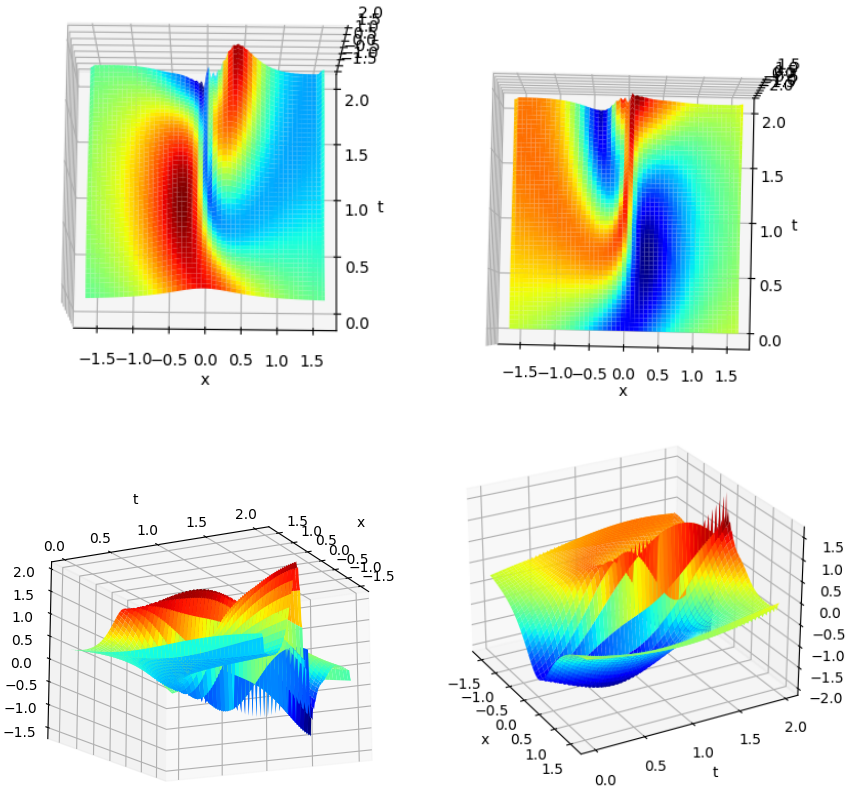

Figure 9: Time evolution of $u(x,t)$ *(left)* and $v(x,t)$ *(right)* using a LF integrator

If we time-evolve the function over longer time periods by increasing the number of timesteps from 200 to 400, but maintain $\Delta t = 0.01$. The system will not blow up, however the solutions becomes less smooth with more spikes. Figure 10 shows exactly this where we have evolved the system with $\alpha = \frac{\pi}{3}$ over 400 timesteps.

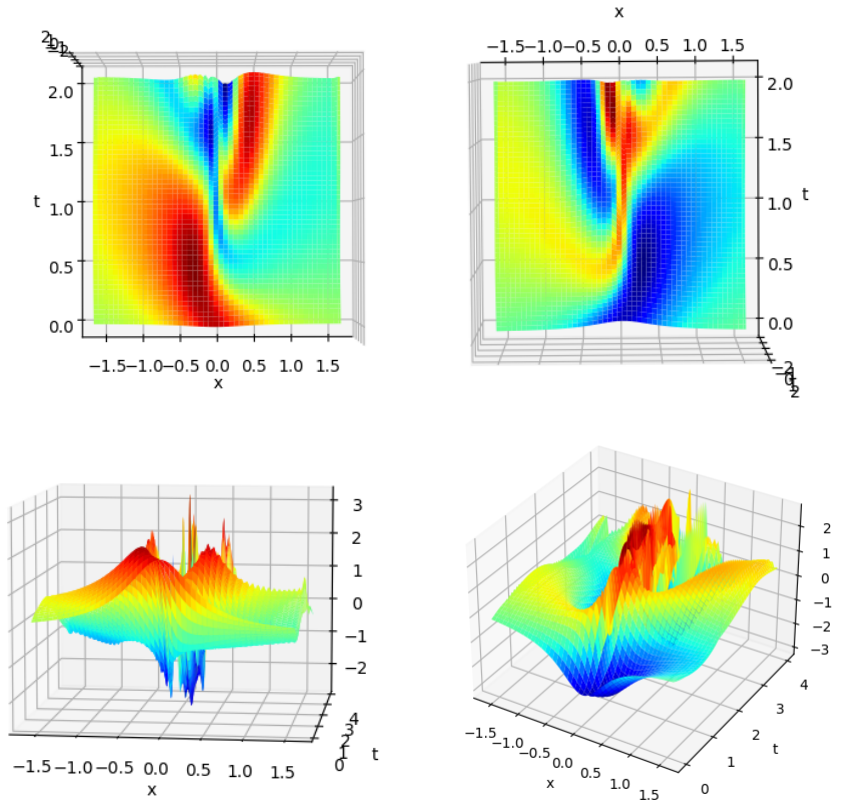

Figure 10: Time evolution of $u(x,t)$ *(left)* and $v(x,t)$ *(right)* using a LF integrator

Evaluating the system shown in Figure 9 for over 400 timesteps shows that the sharpness and frequency of the Spikes increase as time progresses. We know that the approximation of the derivative is subject to error, thus it is likely that the spikes are a result of approximation error and are not characteristics of the systems behaviour. The antisymmetry of the two solutions also vanish as time progresses, since u and v no longer mirror each other after time $t = 2$.

If we increase the value of α and take it to be as large as possible, the system should illustrate many spikes and a breakdown of symmetry. The system with $\alpha = \frac{\pi}{2} - 0.1$ is shown in Figure 11 illustrates both of these points. The anti-symmetry of the waves breaks down when $t = 2$. The spikes alos increase in frequency and magnitude as t gets larger.

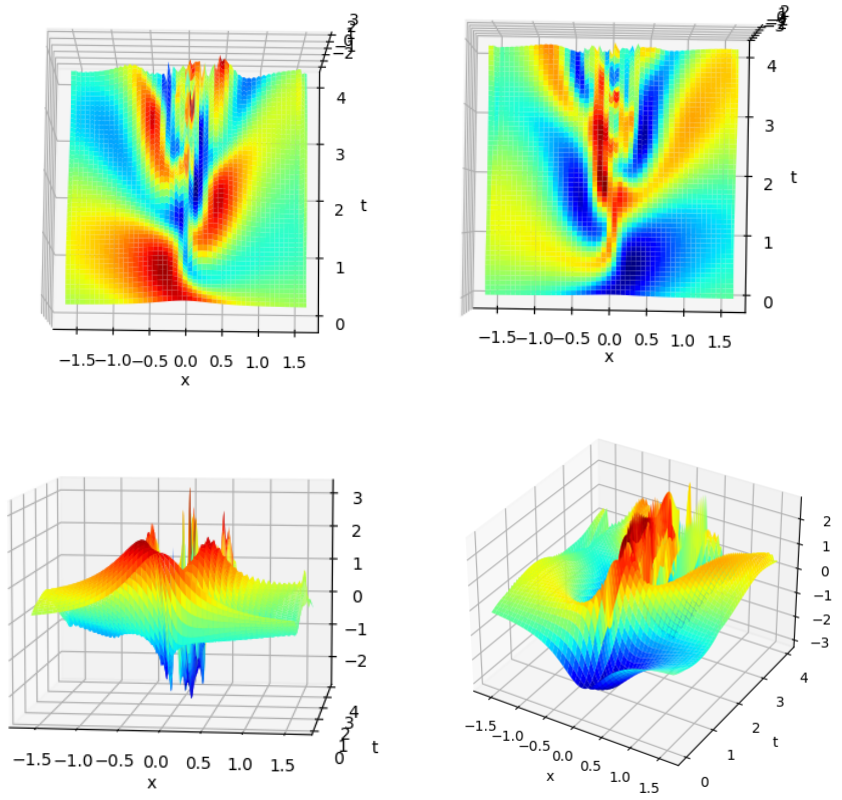

Figure 11: Time evolution of $u(x,t)$ *(left)* and $v(x,t)$ *(right)* using a LF integrator

So far we have only approximated the system described by the Dirac Model (2) where $\frac{\pi}{2} > \alpha > \frac{\pi}{4}$. We will now begin looking at the behaviour of systems with small α If we take $\alpha = 0.5$, figure 11 is produced. This function is entirely smooth, with no spikes. This indicates that the Spikes in the approximated solution is related to large α values only and do not occur for small *alpha*, however further analysis is required to verify this. Both solutions move in opposing directions once again illustrating the antisymmetry of the solutions.

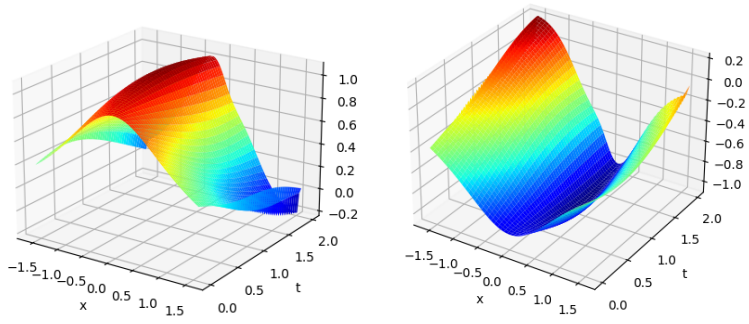

Figure 12: Time evolution of $u(x,t)$ *(left)* and $v(x,t)$ *(right)* using a LF integrator

If we similarly take $\alpha = \frac{\pi}{9}$ and evolve the system over 400 timesteps, the system will maintain its' antisymmetric solution as seen in Figure 12. This contrasts directly with the long term behaviour of the system with $\alpha = \frac{\pi}{2} - 0.1$ shown in figure 11, where the antisymmetry breaks down as t progresses.

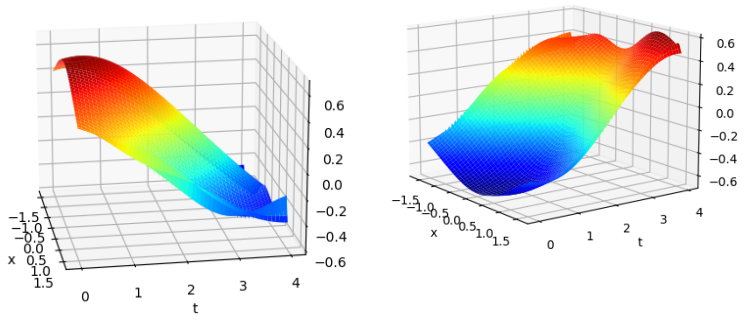

Figure 13: Time evolution of $u(x,t)$ *(left)* and $v(x,t)$ *(right)* using a LF integrator and a Fourier differentiation matrix

The Leapfrog integrator runs in time $\sim 120s$. It is a second order integration method which means the time approximation has an error of the order $O(\Delta t^2)$. It has been shown that the LF integrator produce some spikes in the approximation, resulting in increasingly erratic approximations as the system evolved over time. We will attempt reduce the prevalence of spikes in our approximation by using higher order integrators such as Runge-Kutta 4 (RK4). This allows each approximation to have a more accurate time evolution, which may reduce the spikes in the solution.

4.2 Runge-Kutta 4

Runge Kutta 4 is a popular method used to solve differential equations. Given an equation of the form 20 and the initial conditions of the system ($x(0) = x_0$) the system can be solved easily using this algorithm.

$$\frac{dx}{dt} = f(x,t) \tag{20}$$

The formula for Runge-Kutta 4 is shown in equation 21.

$$\begin{cases} x(\tau+1) = x(\tau) + \frac{1}{6}(k_1 + 2k_2 + 2k_3 + k_4) \\ k_1 = hf(x_\tau, t_\tau) \\ k_2 = hf(x_\tau + \frac{1}{2}h, t_\tau + \frac{1}{2}k_1) \\ k_3 = hf(x_\tau + \frac{1}{2}h, t_\tau + \frac{1}{2}k_2) \\ k_4 = hf(x_\tau + h, t_\tau + k_3) \end{cases} \tag{21}$$

where τ is the time interval between each t value that the system is evaluated at, This formula can be used to time evolve the Spinors according to the Dirac model 2. Figure 14 shows the product of the algorithm when $\alpha = \frac{\pi}{4}$ and timesteps of $\Delta t = 0.01$ are taken 200 times. The Fourier Differentiation Matrix is computed using $N = 100$ x-points as done in the Leapfrog integrator.

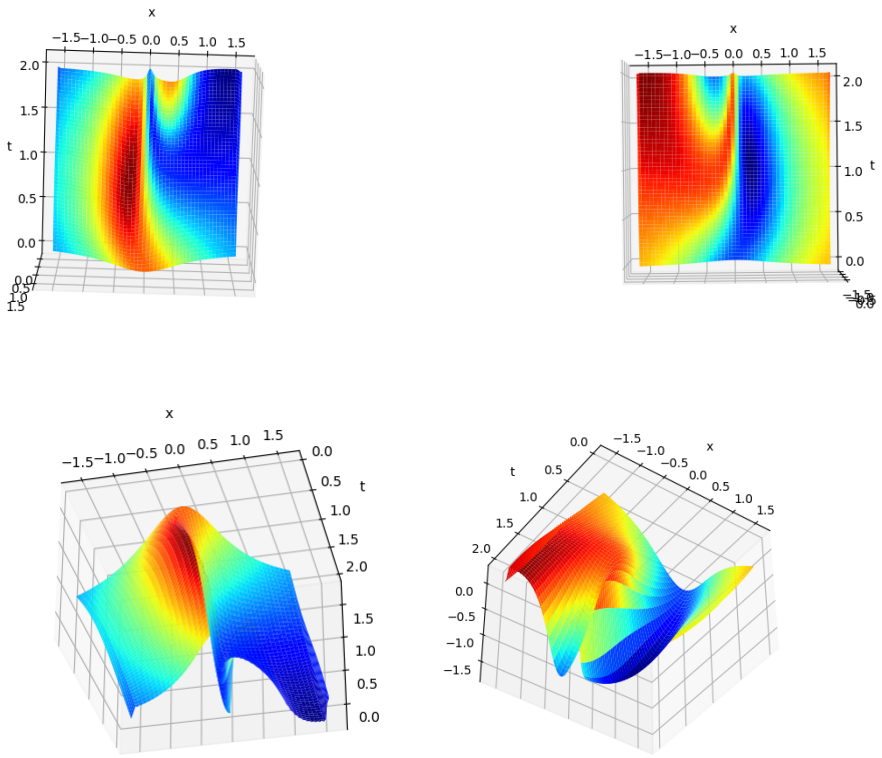

Figure 14: Time evolution of $u(x,t)$ *(left)* and $v(x,t)$ *(right)* using Runge-Kutta

Both spinors solutions are smooth throughout the time evolution. This contrasts Figure 6, which shows spikes where the hump changes from a positive to negative value (or vice versa).
So far, we have gathered an understanding of the solutions u and v when α is large. If we want to understand the behaviour of the system when α is small, we can take $\alpha = \frac{\pi}{10}$ and time-evolve this system. This is shown in Figure 15.

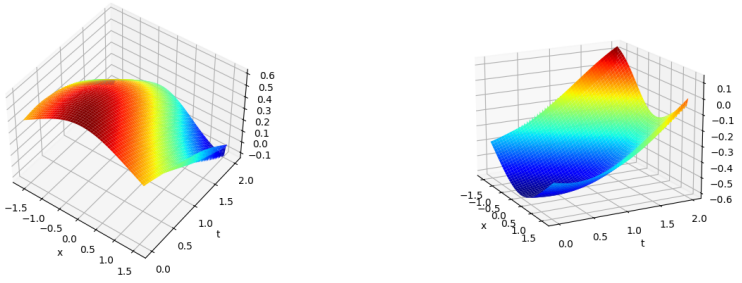

Figure 15: Time evolution of $u(x,t)$ *(left)* and $v(x,t)$ *(right)* using Runge-Kutta and a Fourier differentiation matrix

The hump of the solitons is much smaller and spread out compared to the other figures. This results in a flat looking graph that is difficult to analyse. We will thus take $\alpha = \frac{\pi}{6}$ to analyse the behaviour of the system when α is small.

If we time-evolve the system using RK4 when $\alpha = \frac{\pi}{6}$, the solutions will propagate in different directions as time progresses. This is shown in Figure 15. If we want to analyse the system over longer time periods, we can either increase the number of timesteps or increase the size of each timestep. As shown in the previous section, increasing the size of the timestep can result in the approximation blowing up. This will also occur in the RK4

algorithm at different Δt values. We will maintain that $\Delta t = 0.01$ in this section to maintain stability. The only means to evolve the system over longer time periods is to increase the number of timesteps. Figure 17 shows the same system as Figure 16, just evolved over 400 timesteps instead of 200.

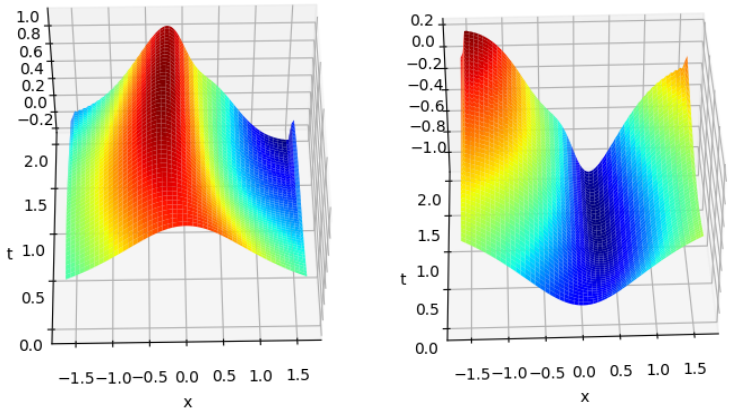

Figure 16: Time evolution of $u(x,t)$ *(left)* and $v(x,t)$ *(right)* using Runge-Kutta and a Fourier differentiation matrix

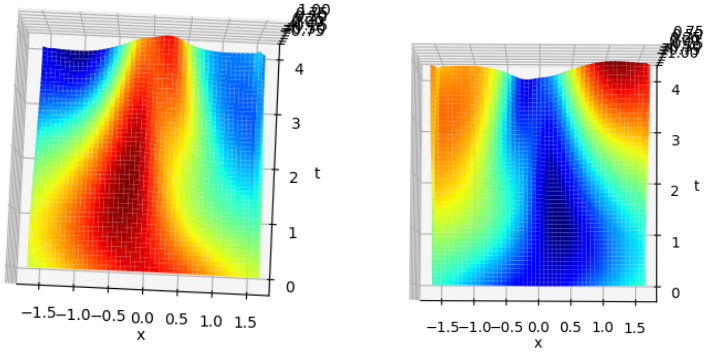

Figure 17: Time evolution of $u(x,t)$ *(left)* and $v(x,t)$ *(right)* using Runge-Kutta 4

Figure 17 illlustrates that even as time progresses, the two solutions will continue to mirror one another. This is in direct contrast to what occurs when $\alpha = \frac{\pi}{3}$. The system behaviour when $\alpha = \frac{\pi}{3}$ is approximated using RK4 in Figure 18. which illustrates a breakdown of the anti-symmetry of the two solutions as time progresses.

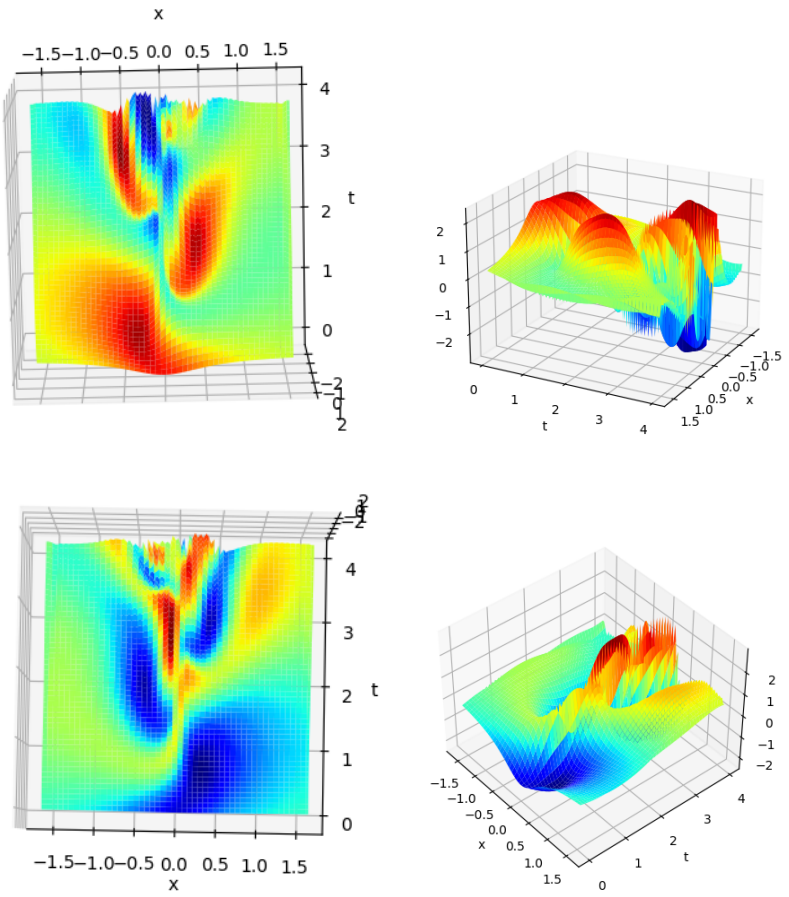

Figure 18: Time evolution of $u(x,t)$ *(left)* and $v(x,t)$ *(right)* using Runge-Kutta and a Fourier differentiation matrix

The Spikes prevalent in the LF approximation of the system similarly appear in the RK4 approximation. In order to compare these spikes we approximate the $\alpha = \frac{\pi}{2} - 0.1$ system using RK4 and compare it to the same system approximated using LF instead. This approximation is shown in Figure 19.

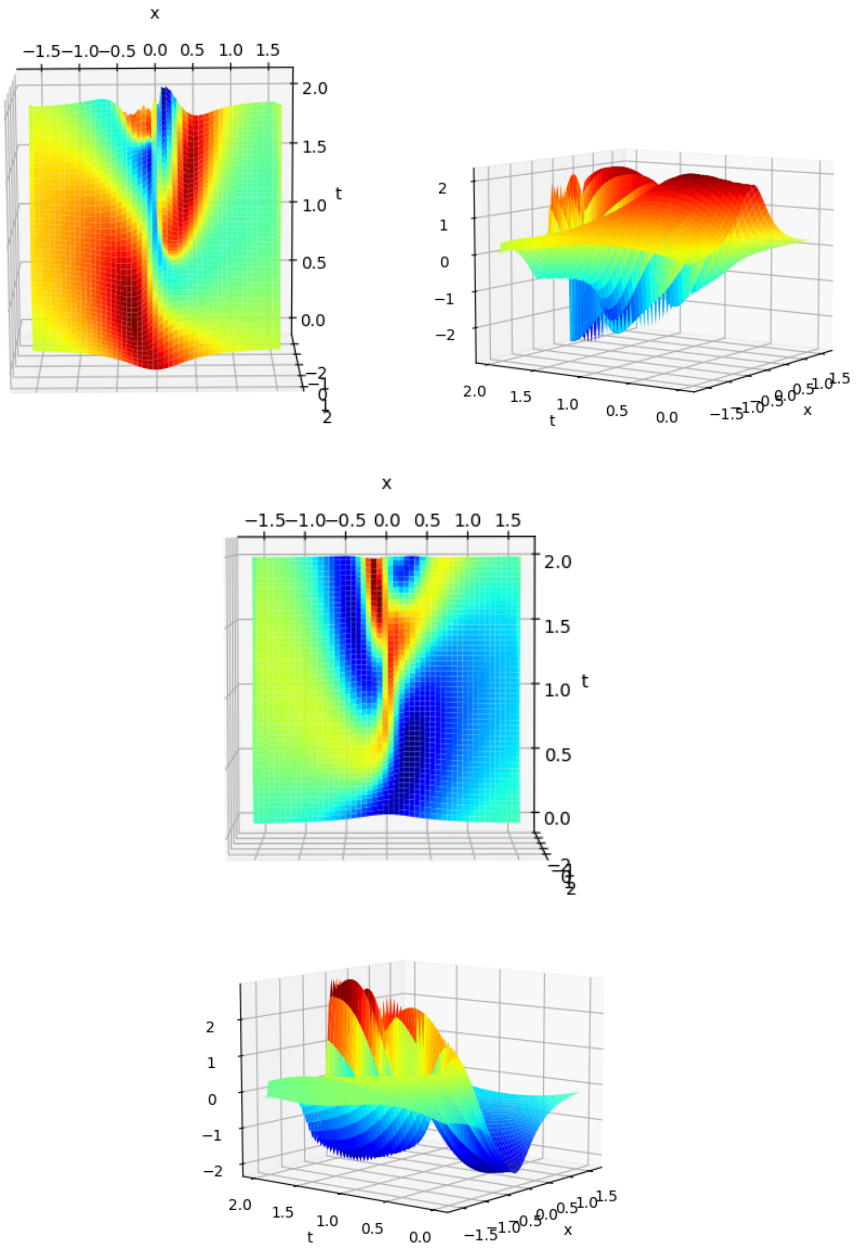

Figure 19: Time evolution of $u(x,t)$ *(left)* and $v(x,t)$ *(right)* using Runge-Kutta and a Fourier differentiation matrix

The Spikes shown in Figure 19 and Figure 11 are produced from a system with $\alpha = \frac{\pi}{2} - 0.1$. These spikes in both approximations become more prevalent as time progresses. The Spikes in the LF integrated system, however, are more frequent and have a larger magnitude. Since both the integrator exhibit the Spikes, it is likely that the system experiences some type of instability as time progresses.

4.3 Computational accuracy and efficiency

Both Integrators were run on python 3.10 using standard packages such as *numpy* and *matplotlib*. Both algorithms will take $\sim 120s$ to run the integrator and plot the resulting time evolution of the system. Both systems presented spikes in the time evolved solutions indicating erratic approximations, however the spikes in the RK4 algorithm were smaller and less frequent compared to the spikes produced by the LF integrator. The Spikes are likely a product of instability in the Dirac model. We will thus analyse the stability of the system in an attempt to understand the errors in the approximate solutions to the system described by the Dirac Model.

4.4 On the behaviour of Spinors

The Spinors u, v are hump-like waves that progress over time via the Dirac Model equations. The waves beat by oscillating between upward humps and downward humps. The behaviour of the humps and of the Spinors themselves will change as parameter α varies.

When the parameter α is small. The beats in the Spinor are barely noticeable. As $\alpha \to \frac{\pi}{4}$ these beats will gradually emerge in both Spinors. u will always begin with an upward beat and v will always begin with a downward one. The humps produces by these beats in wave u will begin moving away from wave v. Wave v will similarly move away from wave u. These waves will beat in sync so u beats upward exactly as v beats downwards.

The in-sync beating and movement of the waves u, v will also occur for $\alpha > \frac{\pi}{4}$. The only difference is that this in sync movement will begin to break down as time progresses. The beats will no longer occur simultaneously and the waves will move in somewhat random directions. This indicates that the waves may become uncoupled for large α, however further analysis of the Dirac model as well as a more in depth understanding of Spinor interactions is required to answer this.

5 Stability of Spinor solutions

The stability of the Spinor solutions can be determined by finding the eigenvalues of the linearised system $A \cdot u_t = \lambda u$, where A is a $N \times N$ matrix. The system will therefore have N eigenvalues denoted λ_i, where $i = 1, 2, 3...N$. The matrix A is shown in figure 17.

where a, b, f, g are the real and imaginary parts of Φ and Ψ. This is shown in equation 22.

$$\begin{aligned} \Phi(x) &= a(x) + ib(x) \\ \Psi(x) &= f(x) + ig(x) \end{aligned} \tag{22}$$

The system will be solved to find eigenvalues λ_i. Recall that the eigenvalues can be used to produce a solution to the linearised problem. The general form of these solution is shown in equation 23 where c_i, d_i are constants to be determined by the Matrix form of specific problems.

$$u(x,t) = \Sigma_{i=1}^{N} c_i e^{d_i \lambda_i t} \tag{23}$$

The solution can be written as a sum of exponentials $e^{\lambda_i t}$. Here we have taken constants $d_i = 1$ for the sake of simplicity although this is often not true in most cases. The exponent will blow up when $Re(\lambda_i) > 0$ since the term will continue to grow as time progresses. When $Re(\lambda) < 0$, the term will converge to some constant. If $Re(\lambda) = 0$ the exponential will evaluate to 1. This produces stability conditions for the Eigenvalues. Foro simplicity we will denote $Re(\lambda) = R_i$

1. The system will be stable if for all λ_i, $R_i < 0$
2. The system will be unstable if for any λ_i, $R_i > 0$
3. If $R_i = 0$, the stability of the system cannot be determined.

If we want to analyse the degree of instability between two unstable systems, the largest R_i of the two systems are compared. The system with a larger R_i value will be more unstable since it will have an exponential term that blows up quicker.

Now that we have all the necessary tools to analyse the stability of the system via its' eigenvalues, we can begin with the system where $\alpha = \frac{\pi}{4}$. This is shown in Figure 19 and Figure 20. The system has Eigenvalues λ_i where $R_i > 0$ and $R_i < 0$. The eigenvalues that lies on the real number line, where $R_i = 0$ are not considered, since these eigenvalues cannot provide any information on the stability of the system.

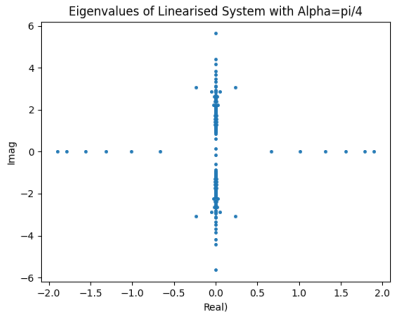

Figure 20: Spectrum of $N = 100$ Eigenvalues

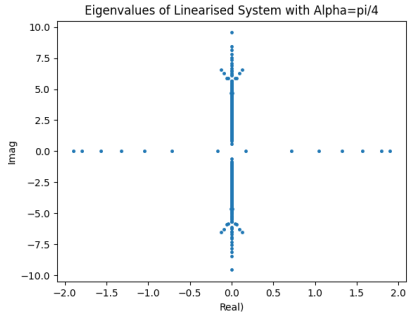

Figure 21: Spectrum of $N = 200$ Eigenvalues

Figure 19 approximates the solution using $N = 100$ x-points. This also results in the Matrix A having dimensions $N \times N$, and consequently N Eigenvalues.Recall that increasing N will increase the accuracy of the approximations. Figure 20 has $N = 200$ which means the approximation will be much better compared to Figure 19 where $N = 100$. The largest $Re(\lambda_i)$ of the system when $N = 100$ is 0.23836 whereas the largest $Re(\lambda_i)$ when $N = 200$ is 0.1277. The System is more unstable when $N = 100$ due to the larger eigenvalue.

α can be varied to understand the influence of this parameter on the stability of the Linearised problem. In the figure below, $N = 100$ and α is varied.

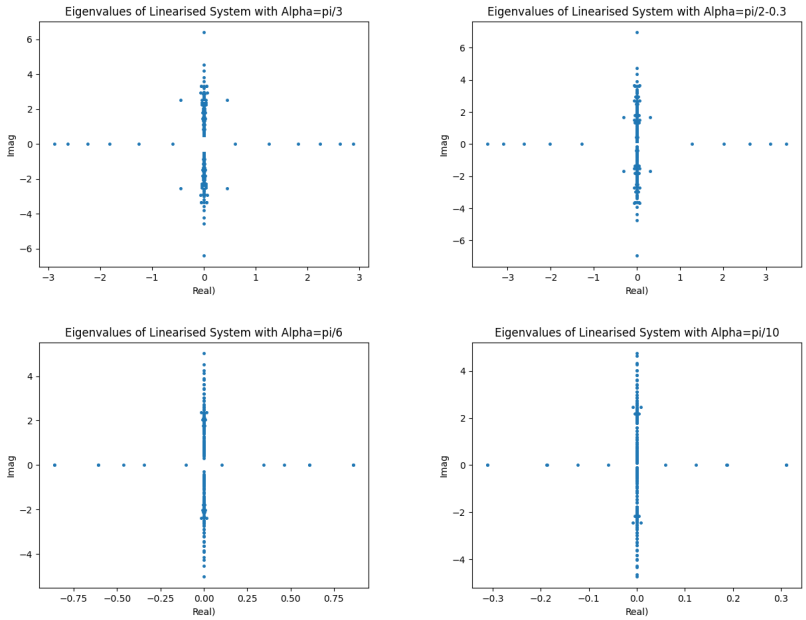

Figure 22: Time evolution of $u(x,t)$ *(left)* and $v(x,t)$ *(right)* using Runge-Kutta and a Fourier differentiation matrix

The R_i decreases in general as $\alpha \to 0$, however it aplso appears to decrease if you get sufficiently close to $\alpha = \frac{\pi}{2}$. The R_i values for the various α values is shown in the table below.

α	R_i
$\frac{\pi}{2} - 0.3$	0.30538
$\frac{\pi}{3}$	0.446538
$\frac{\pi}{4} + 0.15$	0.38489
$\frac{\pi}{4}$	0.23836
$\frac{\pi}{4} - 0.15$	0.04436
$\frac{\pi}{6}$	0.01521
$\frac{\pi}{10}$	0.00847

This indicates that the solution will become more stable as $\alpha \to 0$ or if α is extremely close to $\frac{\pi}{2}$. Note that this does not indicate that the systems are stable. Since for all values of α, there exist $R_i > 0$, the systems will be unstable. The prevalence of the spikes relates directly to the degree of instability in the system. The Spikes are most prevalent in our approximated solution when $\alpha = \frac{\pi}{3}$ and $\alpha = \frac{\pi}{4}$, which corresponds to the two largest R_i values in the table. It is important to note that the R_i values are still small since they are all less than one, indicating that the solutions will take a long time to become unstable. The solutions are therefore considered long-lived but not stable.

6 Conclusion

The Nonlinear Dirac Model 2 has Stationary state solutions known as Spinors Φ, Ψ that can be evolved over time using the time operator e^{-iwt} as shown above. The nonlinearity of the system means the system is not easily solved, since both solution u, v must be calculated at each timestep. This will result in incredibly long computations. Alternatively numeric methods can be used to time-evolve the systems over time.

Spectral methods have been shown to be incredibly accurate and simple. In this paper we have outlined two methods approximate the Derivative of a function as well as their uses. The Chebyshev Differentiation

matrix can be used when studying stationary state solutions, but not time evolutions solutions since these approximations will blow up. When evolving a solution over time, the Fourier Differentiation matrix is preferred. Although it is less accurate, the approximations will not blow up. This Fourier Differentiation matrix is thus used to time-evolve the Spinors to get the full solution to the Dirac Model.

The systems are evolved over time using one symplectic and one non-symplectic integrator, namely Leapfrog and Runge-Kutta 4. RK4 provides smoother approximations by reducing the prevalence of erratic spikes as the system progresses over time. The RK4 algorithm is therefore the preferred method when numerically approximating solutions to the Dirac Model.

Stability analysis of the linearized system shows that the system is unstable for all α values, however the solutions are long-lived before they become unstable. The unstableness of the system is likely the cause of the spikes in the time evolved system. All the systems may therefore produce waves u, v that eventually move randomly and beat out-of-sync as time progresses.

The solutions to the nonlinear Dirac Model can be approximated numerically using Spectral methods and time integrators. The resulting approximations will grow increasingly unstable as time progresses. The instability of the system however, is incredibly slow, allowing the solitary wave solutions to propogate for extremely long periods before breaking down.

7 References

1. Admin (2022) Runge Kutta RK4 Method: Fourth order runge kutta method, BYJUS. BYJU'S. Available at: https://byjus.com/maths/runge-kutta-rk4-method/ (Accessed: April 29, 2023).

2. Alexeeva, N.V., Barashenkov, I.V. and Saxena, A. (2019) "Spinor solitons and their PT-symmetric offspring," Annals of Physics, 403, pp. 198–223. Available at: https://doi.org/10.1016/j.aop.2018.11.010.

3. Trefethen, L.N. (2000) Spectral methods in MATLAB. Philadelphia, Pa: Society for Industrial and Applied Mathematics.

4. Xu, J., Shao, S. and Tang, H. (2013) "Numerical methods for nonlinear Dirac equation," Journal of Computational Physics, 245, pp. 131–149. Available at: https://doi.org/10.1016/j.jcp.2013.03.031.

8 Appendix: Codes

All Codes in this paper can be found on the Github link: https://github.com/qiulinlx/DiracSolitons